Supporting Information

A robust 3D zinc(II)–organic framework for efficient dual detection of acetylacetone and Tb^{3+} ions

Miao-Miao Fu[a], Lianshe Fu[b], Guang-Hua Cui[a]*

[a]*College of Chemical Engineering, Hebei Key Laboratory for Environment Photocatalytic and Electrocatalytic Materials, North China University of Science and Technology, No. 21 Bohai Road, Caofeidian new-city, Tangshan, Hebei, 063210, P. R. China*

[b]*Department of Physics and CICECO-Aveiro Institute of Materials, University of Aveiro, 3810-193 Aveiro, Portugal*

*Corresponding author: Guang-Hua Cui;

Fax: +86–315–8805462. Tel: +86–315–8805460

E-mail: tscghua@126.com.

CONTENTS

Section 1. Experimental Section

1. Crystal synthesis experiments
2. Stability experiments
3. Sensing experiments
4. Electrochemical measurement

1. Crystal synthesis experiments

Dissolve L, $Zn(OAc)_2 \cdot 2H_2O$ and H_2DCTP in 10 mL H_2O according to a molar ratio of 1: 3: 3 and seal in a 25 mL Teflon-lined stainless steel container after ultrasonication for 10 minutes. The slurry was heated at 140 °C for 3 days, then cooled to room temperature at a rate of 10 °C/h. After obtaining bulk crystals, the crystals were collected with the Rigaku XtaLabMini diffractometer and refined with full matrix least square method based on F^2 using SHELXL-2018 program. Finally, the product and well-resolved crystal structure data were obtained.

2. Stability experiments

4 mg **1** after finely grinding was dispersed into 4 mL several organic solvents, including H_2O, MeOH (methanol), NBA (n-butanol), EtOH (ethanol), NMP (N-methyl pyrrolidone), DMF (N, N-dimethylformamide), DMSO (dimethyl sulfoxide), MeCN (acetonitrile), DCM (dichloromethane), CHX (cyclohexane) and acac, then the suspension was sonicated for 30 min and soaked for 24 h, washed and dried for PXRD experiment to evaluate the stability of **1** in the several solvents. The pH buffer solution (pH = 3–12) is prepared by adjusting the ratio of glacial acetic acid and sodium acetate trihydrate. Then add 4 mg of evenly ground powder **1** to 4 mL of different pH solutions, and standing for 30 min at room temperature to infiltrate it completely. Then, the fluorescence intensity experiment of the complex **1** was carried out. Finally, the sample was washed and dried for PXRD measurements to evaluate the stability of **1** toward different pH solutions.

3. Sensing experiments

The finely ground powder **1** (4 mg) was immersed in various organic solvents (4 mL) (see **stability experiments section** for details). After ultrasonic treatment for 30 min, the fluorescence emission of **1** in different solvent were explored. For metal ion sensing, 4 mg powder and 4 mL

ethanol/water mixed solvents (volume ratio=1:1) containing $M(NO_3)_x$ (0.001 mol L^{-1}, M = Na^+, K^+, Ca^{2+}, Sr^{2+}, Ba^{2+}, Cr^{3+}, Fe^{3+}, Co^{2+}, Ni^{2+}, Zn^{2+}, Ag^+, Cd^{2+}, Hg^{2+}, Al^{3+}, Pb^{2+}, La^{3+}, Gd^{3+}, and Tb^{3+}) to form homogeneous suspensions for photoluminescence measurement. The solvent and ion anti-interference experiments were carried out. The suspension was formed by adding complex **1** in the presence of acac (2 mL) and other organic solvents (2 mL) after sonication for 30 minutes, and then the fluorescence intensity was tested. Competitive testing is performed in the presence of other various metal ions and Tb^{3+} ions. Add 0.1 mL, 0.001 M Tb^{3+} ions and 1.9 mL ethanol solution to 2 mL of other ions with a concentration of 0.001 M, the concentration of Tb^{3+} ions is lower than other ions. The time-dependent fluorescence emission response spectra for **1** were also further measured. After adding acac/Tb^{3+} with a concentration of $4.0/1.0\times10^{-3}$ mol/L to **1**, the fluorescence intensity was measured every 5 s, and record the time required to reach a stable value.

4. Electrochemical measurement

A CHI660E electrochemical workstation (Chenhua, Shanghai, China) was employed to investigate the cyclic voltammogram (CV) of **1** in the 0.1 mol L^{-1} Na_2SO_4 aqueous solutions. A glassy carbon electrode (GCE, Ø = 3 mm) was coated with **1** as follows: 24 mg powder of **1** was ultrasonicated in 4 mL ethanol for 2 h. Then, 30 μL of the suspension was placed on the surface of the GCE and dried in air for 30 min at room temperature. After that, 10 μL of 0.2% Nafion solution was transferred quantitatively onto the surface of the modified GCE. Finally, the **1**/GCE was obtained after drying in air for about 1 h. The modified **1**/GCE, saturated calomel electrode (SCE), and platinum electrode were applied as the working electrode, reference electrode, and auxiliary electrode, respectively. The electrochemical behavior of **1** was evaluated by CV technique with the scan rate of 50 mV s^{-1}.

Section 2. Supplementary Scheme, Tables and Figures

Scheme Titles:

Scheme S1. The structural formula of the ligands.

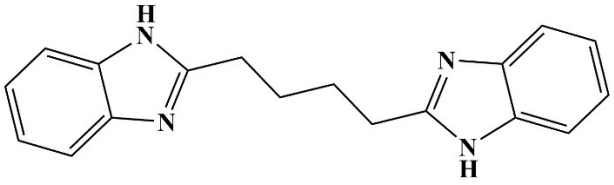

L = 1,4-di(1*H*-benzo[*d*]imidazol-2-yl)butane

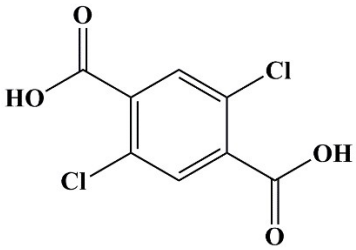

H_2DCTP = 2,5-dichloroterephthalic acid

Scheme 1. The structural formula of the ligands.

Table Titles:

Table S1. Crystallographic data and refinement parameter for **1**.

Table S2. Selected bond lengths (Å) and angles (°) for **1**.

Table S3. HOMO-LUMO energies (in eV) for **1** and acac.

Table S1 Crystallographic data and refinement parameter for **1**

CPs	**1**
Chemical formula	$C_{42}H_{24}Cl_6N_4O_{12}Zn_3$
Formula weight	1185.46
Crystal system	Triclinic
Space group	$P\bar{1}$
a (Å)	9.78(2)
b (Å)	13.53(3)
c (Å)	18.31(3)
α (°)	81.65(2)
β (°)	84.86(2)
γ (°)	70.36(2)
V (Å^3)	2255.68(9)
Z	2
D_{calcd} (g/cm^3)	1.745
Absorption coefficient, mm^{-1}	2.005
F(000)	1184
Crystal size, mm	0.22×0.18×0.16
θ range, *deg*	3.694–61.2
Index range h, k, l	−13/13, −19/19, −25/25
Reflections collected	65961
Independent reflections (R_{int})	13170(0.0497)
Data/restraint/parameters	13170 / 0 / 607
Goodness-of-fit on F^2	1.016
Final R_1, wR_2 ($I > 2\sigma(I)$)	0.0471, 0.0827
Largest diff. peak and hole	1.46, −0.89

Table S2 Selected bond lengths (Å) and angles (°) for **1**

Parameter	Value	Parameter	Value
Zn(3)–O(11)	2.044(2)	Zn(3)–O(2)A	1.982(2)
Zn(3)–O(9)	1.984(2)	Zn(3)–O(12)	2.481(2)
Zn(4)–O(11)	2.254(2)	Zn(4)–O(10)	2.018(2)
Zn(4)–O(11)B	2.254(2)	Zn(4)–O(10)B	2.019(2)
Zn(4)–O(1)A	2.025(2)	Zn(2)–O(6)	1.986(2)
Zn(2)–O(4)	1.959(2)	Zn(2)–O(7)	3.1039(14)
Zn(1)–O(6)	2.286(2)	Zn(1)–O(8)	1.992(2)
Zn(1)–O(3)	2.019(2)	Zn(3)–N(4)	1.986(2)
Zn(2)–N(2)	1.990(2)	O(11)–Zn(3)–O(12)	56.96(7)
O(2)A–Zn(3)–O(11)	111.18(8)	O(2)A–Zn(3)–O(9)	113.52(9)
O(2)A–Zn(3)–O(12)	90.41(8)	O(9)–Zn(3)–O(11)	97.89(8)
O(9)–Zn(3)–O(12)	151.27(8)	O(11)–Zn(4)–O(11)B	180.00(9)
O(10)B–Zn(4)–O(11)	90.28(8)	O(10)–Zn(4)–O(11)	89.72(8)
O(10)–Zn(4)–O(11)B	90.28(8)	O(10)B–Zn(4)–O(11)B	89.72(8)
O(10)–Zn(4)–O(10)B	180.00(5)	O(10)–Zn(4)–O(1)A	93.50(8)
O(10)B–Zn(4)–O(1)A	86.50(8)	O(10)–Zn(4)–O(1)C	86.50(8)
O(10)B–Zn(4)–O(1)C	93.50(8)	O(1)A–Zn(4)–O(11)	87.23(7)
O(1)A–Zn(4)–O(11)B	92.76(2)	O(1)C–Zn(4)–O(11)B	87.24(7)
O(1)C–Zn(4)–O(11)	92.77(7)	O(1)C–Zn(4)–O(1)A	180.00(7)
O(4)–Zn(2)–O(6)	109.30(8)	O(4)–Zn(2)–O(7)	112.81(10)
O(7)–Zn(2)–O(6)	96.88(8)	O(6)D–Zn(1)–O(6)	180.0
O(8)–Zn(1)–O(6)	95.50(8)	O(8)–Zn(1)–O(6)D	84.50(8)
O(8)D–Zn(1)–O(6)D	95.50(8)	O(8)D–Zn(1)–O(6)	84.50(8)
O(8)–Zn(1)–O(8)D	180.0	O(8)D–Zn(1)–O(3)	86.12(11)
O(8)–Zn(1)–O(3)D	86.12(11)	O(8)–Zn(1)–O(3)	93.88(11)
O(8)D–Zn(1)–O(3)D	96.88(11)	O(3)–Zn(1)–O(6)	91.65(8)
O(3)D–Zn(1)–O(6)	88.35(8)	O(3)–Zn(1)–O(6)D	88.35(8)
O(3)D–Zn(1)–O(6)D	91.65(8)	O(3)–Zn(1)–O(3)D	180.00(15)
O(2)A–Zn(3)–N(4)	115.38(9)	O(9)–Zn(3)–N(4)	96.95(9)
N(4)–Zn(3)–O(11)	119.46(8)	N(4)–Zn(3)–O(12)	85.96(8)
N(2)–Zn(2)–O(6)	127.37(9)	Zn(2)–O(6)–Zn(1)	98.90(7)
Zn(3)–O(11)–Zn(4)	99.89(7)		

symmetry code: A: *x*, *y*, 1+*z*, B: 1−*x*, 2−*y*, 2−*z*, C: 1−*x*, 2−*y*, 1−*z*, D: −*x*, 2−*y*, 1−*z*, E: 2−*x*, 2−*y*, 2−*z*, F: −1−*x*, 2−*y*, 1−*z*, G: 1−*x*, 1−*y*, 2−*z*, H: 1−*x*, 1−*y*, 1−*z* for **1**.

Table S3. HOMO-LUMO energies (in eV) for **1** and acac

types	HOMO	LUMO
1	–5.06	–1.63
acac	–4.93	–2.36

Figure Titles:

Fig. S1. Geometric coordination configuration of four Zn metal centers for **1**.

Fig. S2. Two trinuclear Zn(II) SBUs of **1**.

Fig. S3. Two 1D chains along *c* and *a*-axis formed by modes **I** (top-left) and **II** (top-right).

Fig. S4. 1D V-shaped chain along *b*-axis formed by mode **III**.

Fig. S5. SEM image of **1**.

Fig. S6. Simulated and experimental PXRD patterns for **1**.

Fig. S7. TGA curve of **1**.

Fig. S8. PXRD pattern of **1** soaked in different organic solvents.

Fig. S9. PXRD pattern of **1** soaked in aqueous solution of different pH.

Fig. S10. Time-dependent fluorescence response of **1** toward acac.

Fig. S11. Anti-interference experiment of acac in **1** to different solvents.

Fig. S12. Stern-Volmer curves of **1** in aqueous solutions with different concentrations of acac (Inset: Corresponding linear relationship of **1**).

Fig. S13. Three cycles experiment to identify acac in **1**.

Fig. S14. PXRD pattern after three cycles of sensing acac of **1**.

Fig. S15. UV–Vis spectra of various organic solvents and excitation spectra of **1**.

Fig. S16. Time-dependent fluorescence response of **1** toward Tb^{3+} ions.

Fig. S17. Influence of interfering ions on the luminescence intensity of Tb^{3+} ions.

Fig. S18. Three cycles experiment to identify Tb^{3+} ions in **1**.

Fig. S19. PXRD patterns of **1** after three cycles of sensing Tb^{3+} ions.

Fig. S20. Luminescence decay curves. (a) τ = 2.66 μs for **1**, (b) τ = 2.15 μs for **1** with a load of 0.001 M Tb^{3+} ions.

Fig. S21. (a) TEM image of **1**, (b) EDS-mapping images of C, N, O, Cl, Zn and Tb in **1** after sensing Tb^{3+} ions.

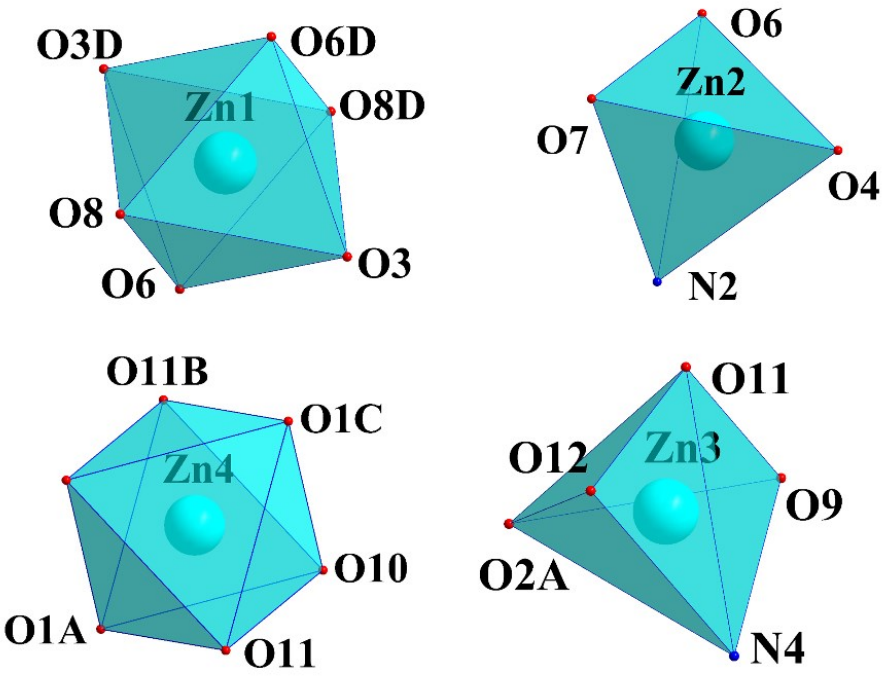

Fig. S1. Geometric coordination configuration of four Zn metal centers for **1**.

(symmetry code: A: *x*, *y*, 1+*z*, B: 1−*x*, 2−*y*, 2−*z*, C: 1−*x*, 2−*y*, 1−*z*)

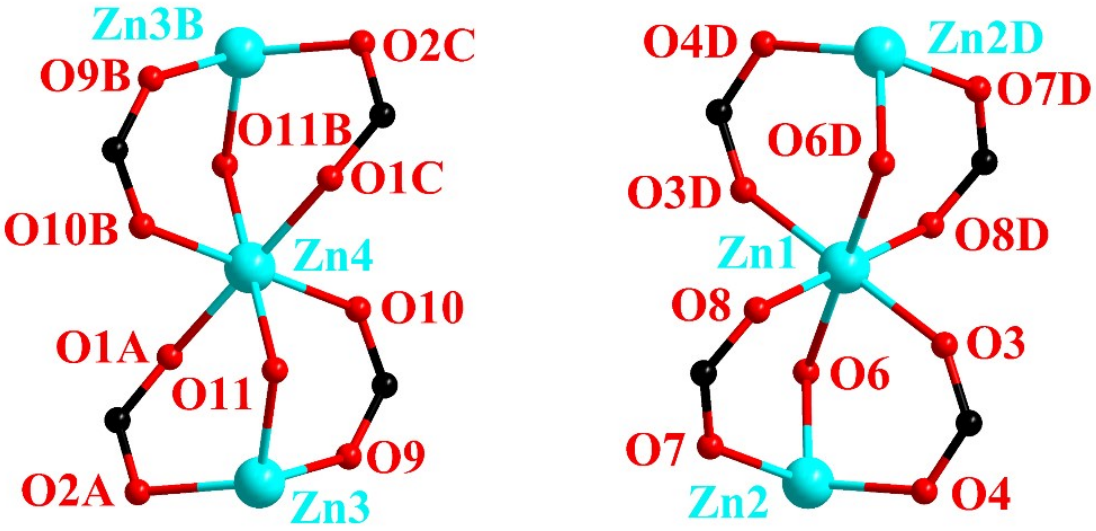

Fig. S2. Two trinuclear Zn(II) SBUs of **1**.

(symmetry code: A: *x*, *y*, 1+*z*, B: 1−*x*, 2−*y*, 2−*z*, C: 1−*x*, 2−*y*, 1−*z*, D: −*x*, 2−*y*, 1−*z*)

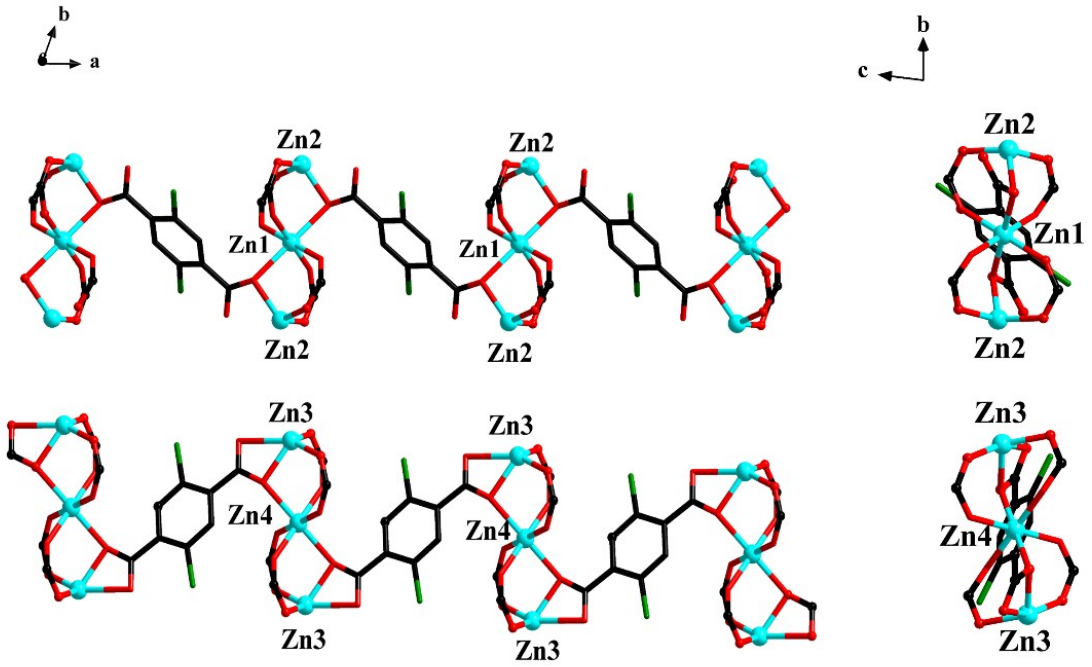

Fig. S3. Two 1D chains along *c* and *a*-axis formed by modes **I** (top-left) and **II** (top-right).

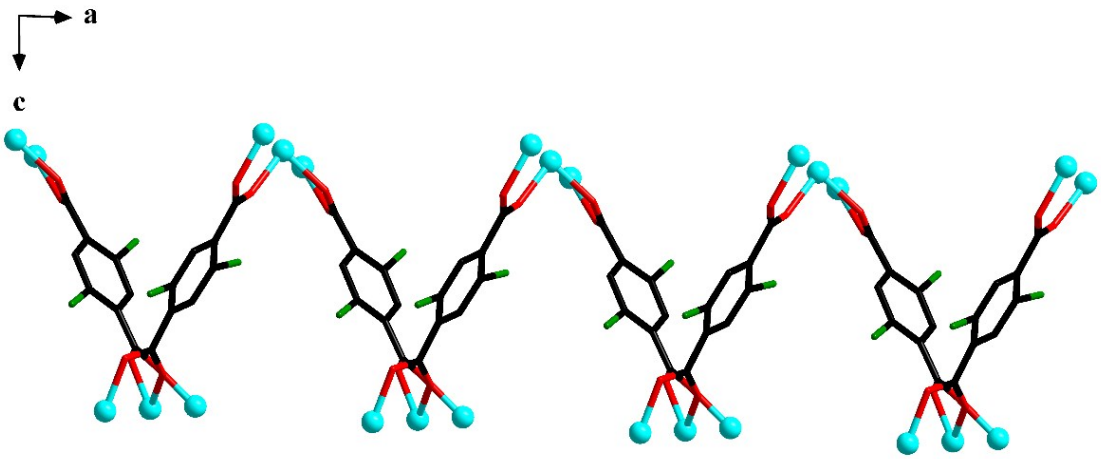

Fig. S4. 1D V-shaped chain along *b*-axis formed by mode **III**.

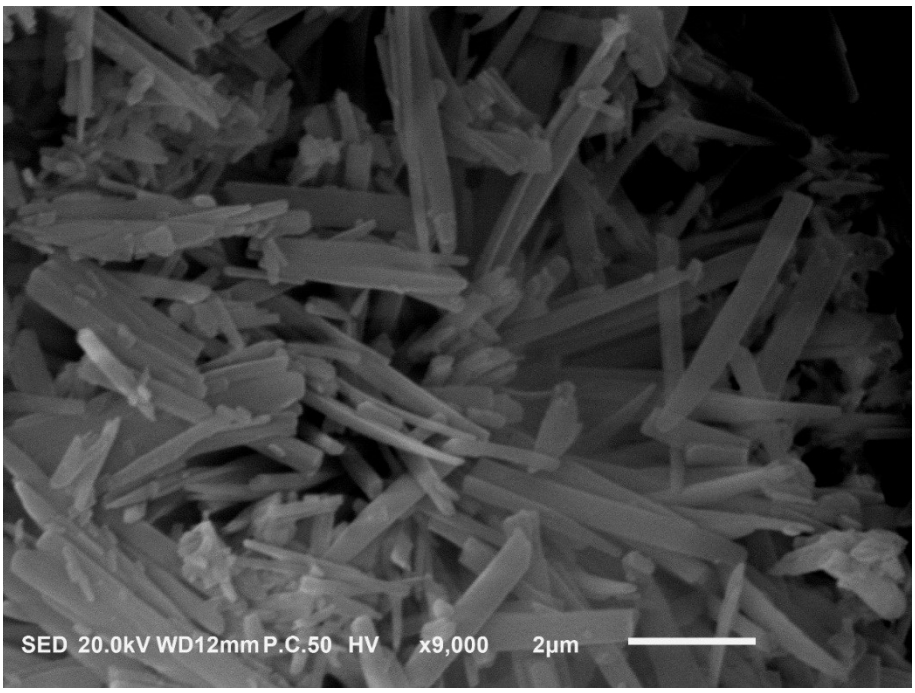

Fig. S5. SEM image of **1**.

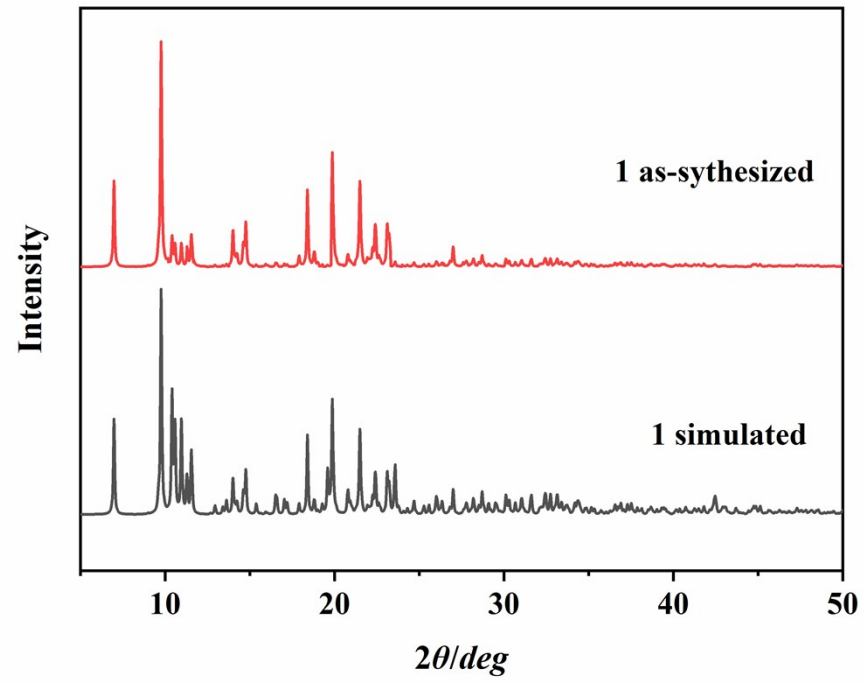

Fig. S6. Simulated and experimental PXRD patterns for **1**.

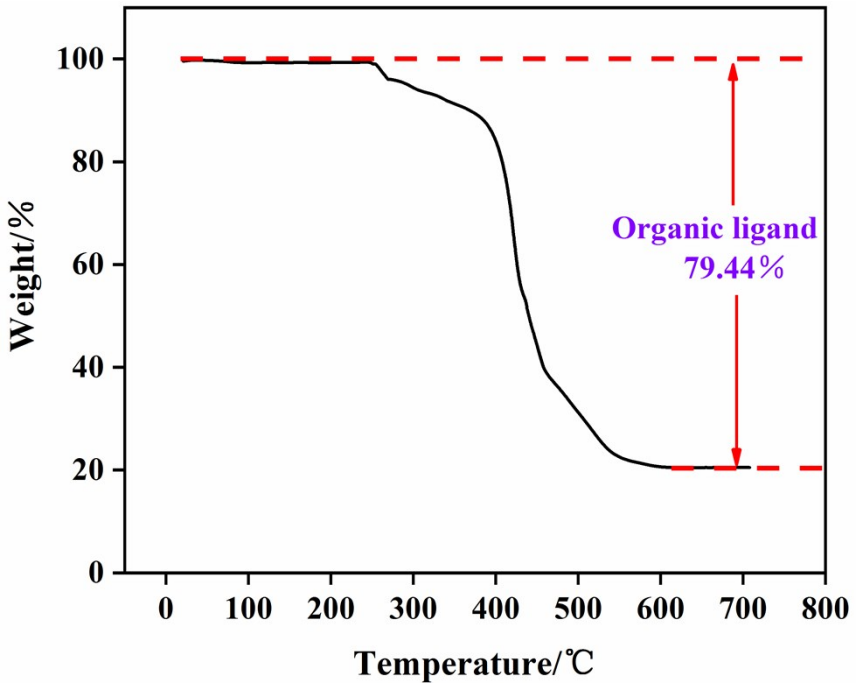

Fig. S7. TGA curve of **1**.

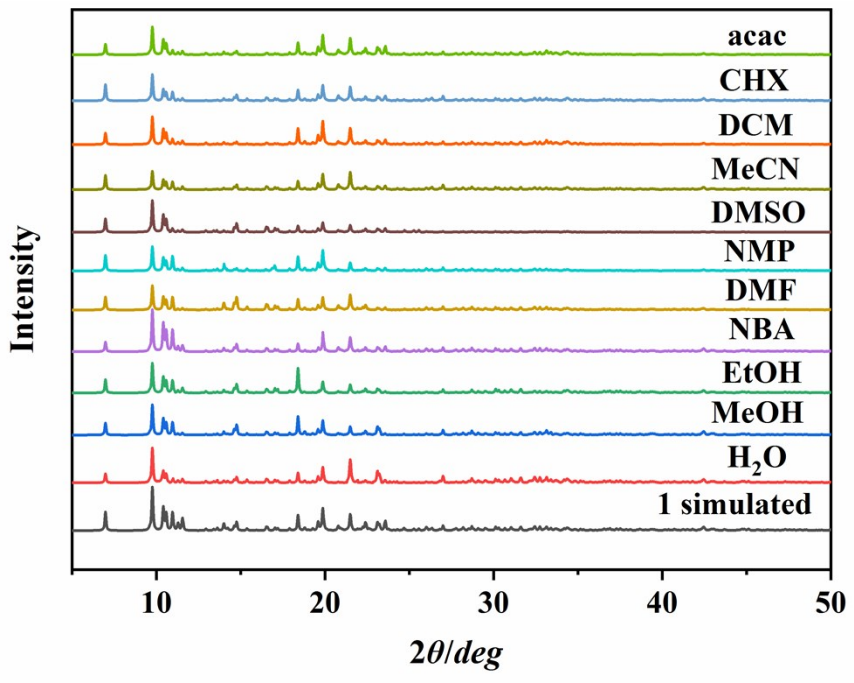

Fig. S8. PXRD pattern of **1** soaked in different organic solvents.

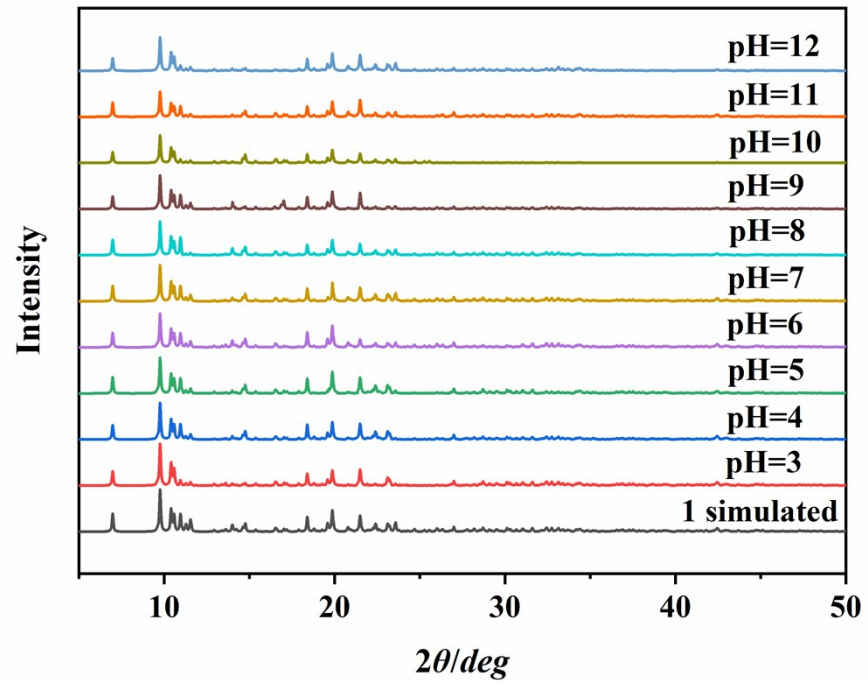

Fig. S9. PXRD pattern of **1** soaked in aqueous solution of different pH.

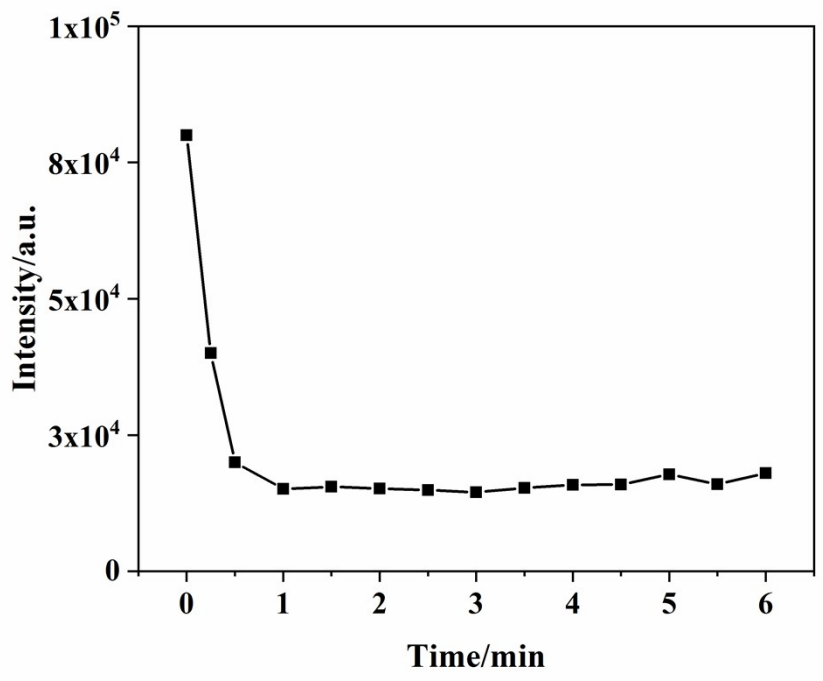

Fig. S10. Time-dependent fluorescence response of **1** toward acac.

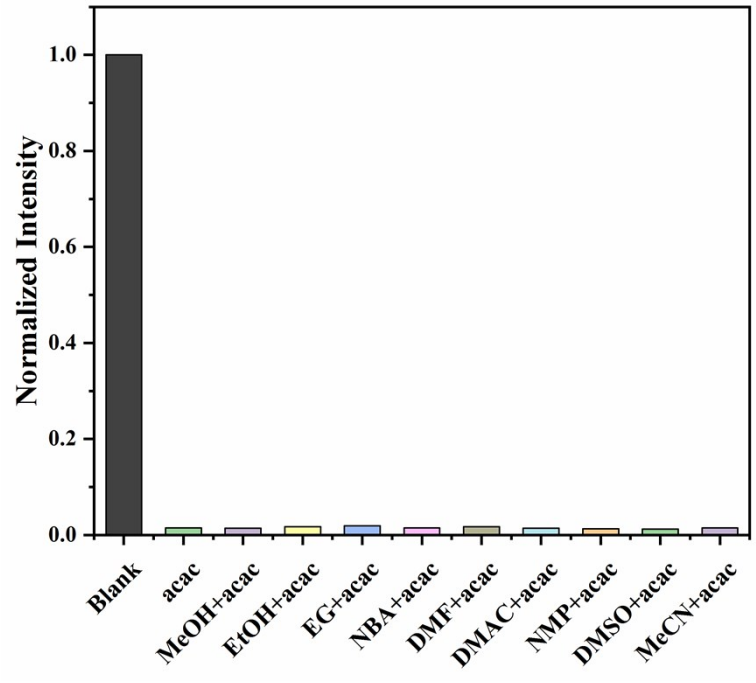

Fig. S11. Anti-interference experiment of acac in **1** to different solvents.

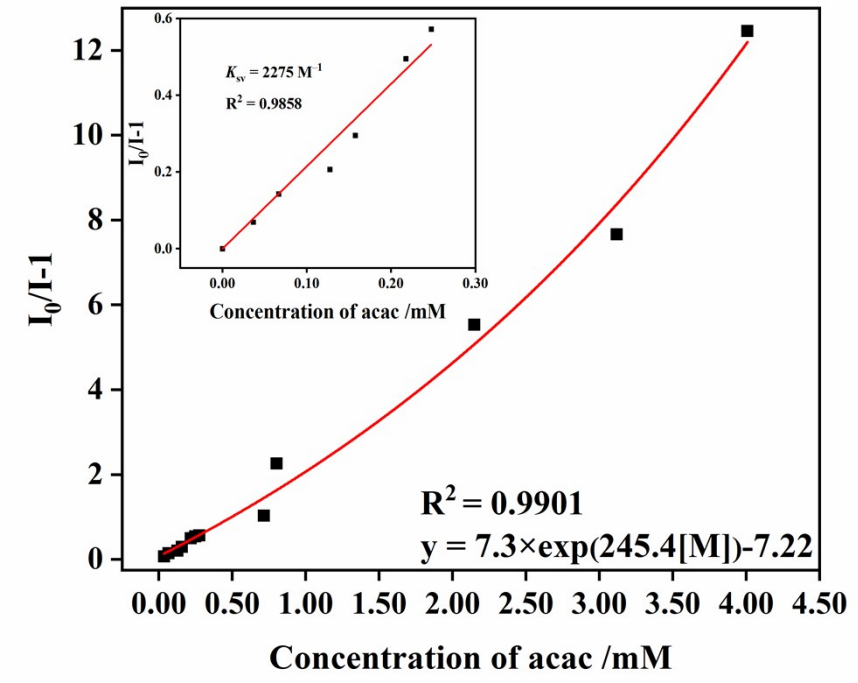

Fig. S12. Stern-Volmer curves of **1** in aqueous solutions with different concentrations of acac (Inset: Corresponding linear relationship of **1**).

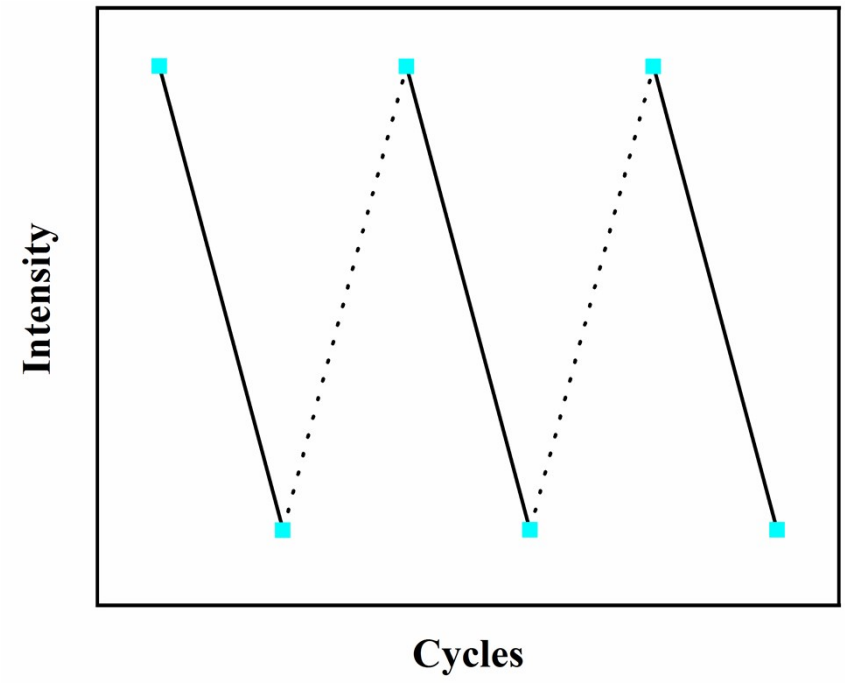

Fig. S13. Three cycles experiment to identify acac in **1**.

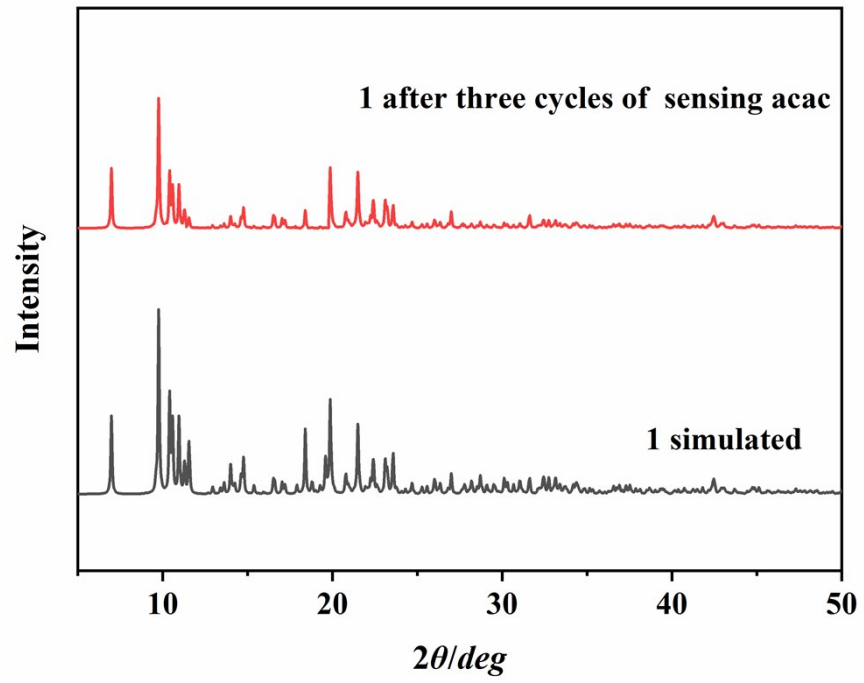

Fig. S14. PXRD pattern after three cycles of sensing acac of **1**.

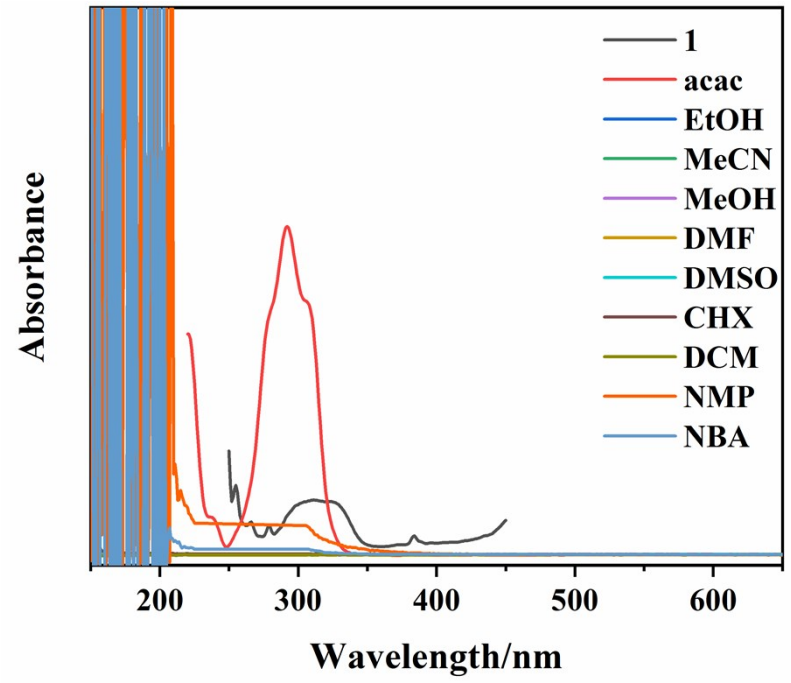

Fig. S15. UV–Vis spectra of various organic solvents and excitation spectra of **1**.

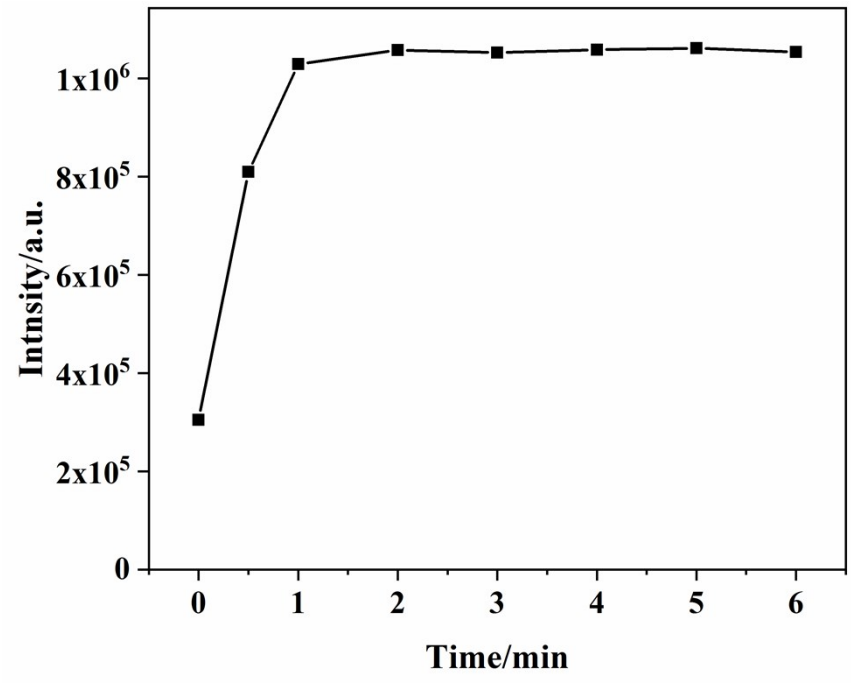

Fig. S16. Time-dependent fluorescence response of **1** toward Tb^{3+} ions.

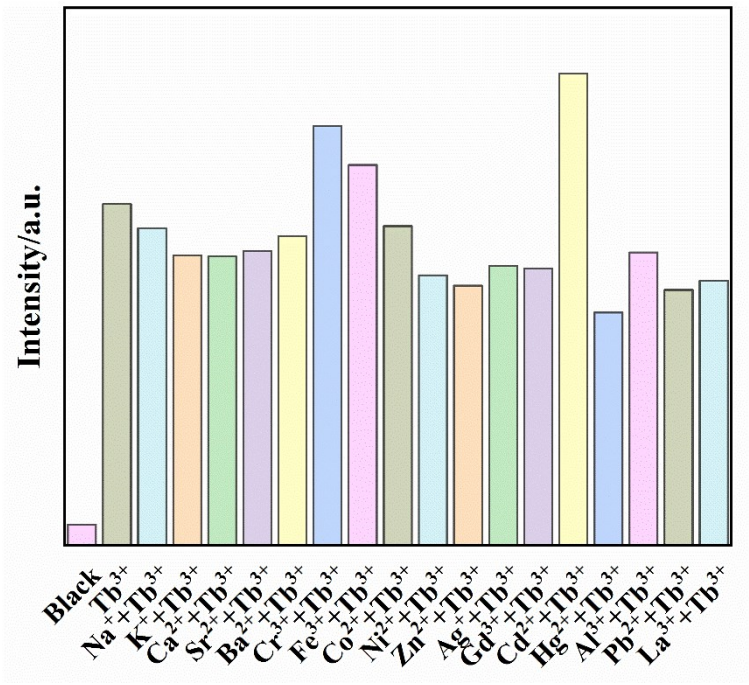

Fig. S17. Influence of interfering ions on the luminescence intensity of Tb^{3+} ions.

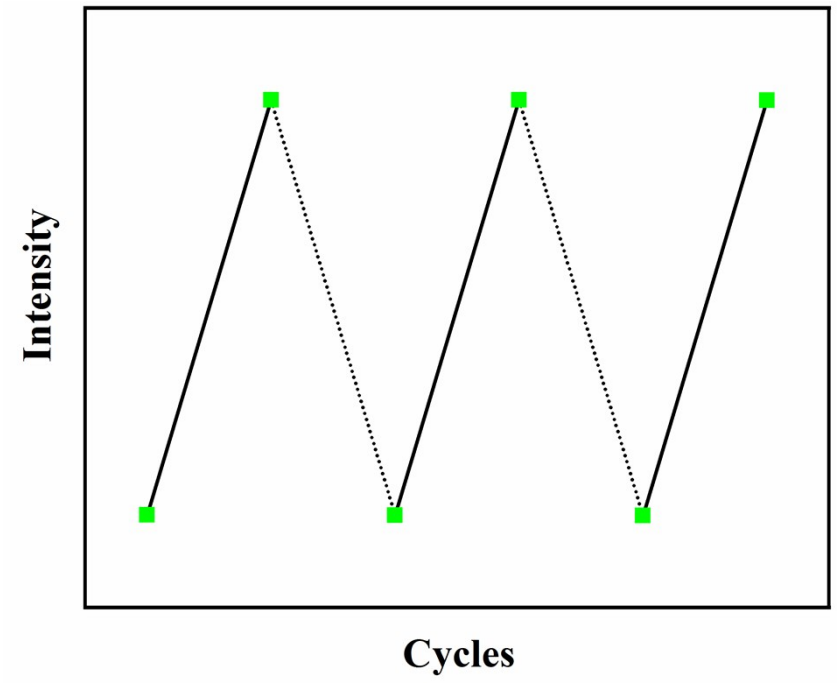

Fig. S18. Three cycles experiment to identify Tb^{3+} ions in **1**.

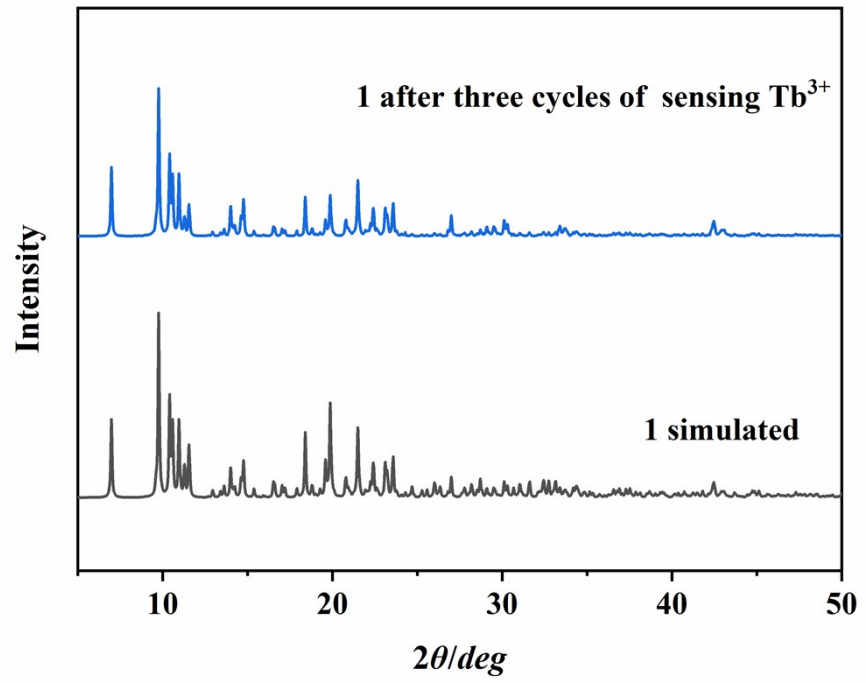

Fig. S19. PXRD patterns of **1** after three cycles of sensing Tb^{3+} ions.

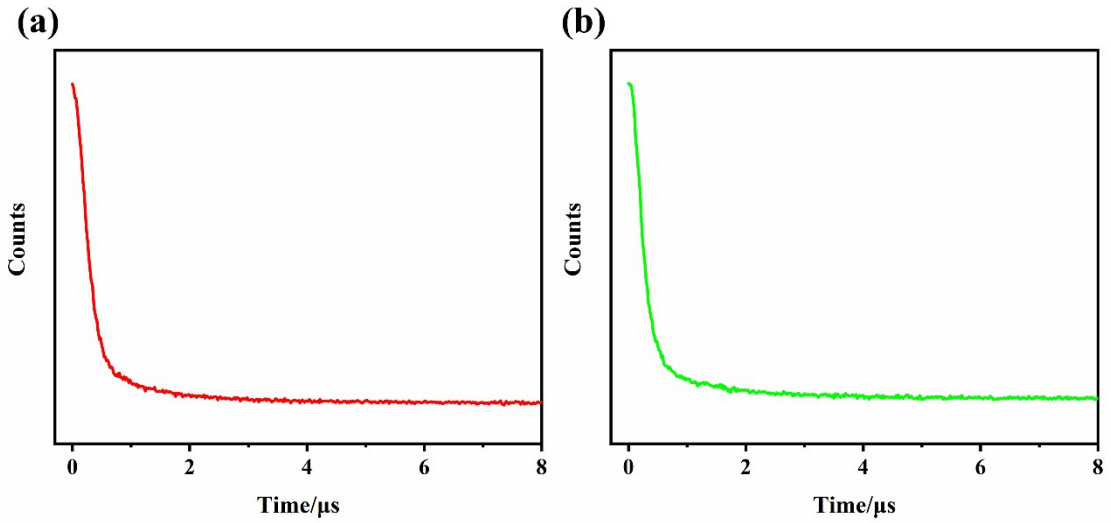

Fig. S20. Luminescence decay curves. (a) τ = 2.66 μs for **1**, (b) τ = 2.15 μs for **1** with a load of 0.001 M Tb^{3+} ions.

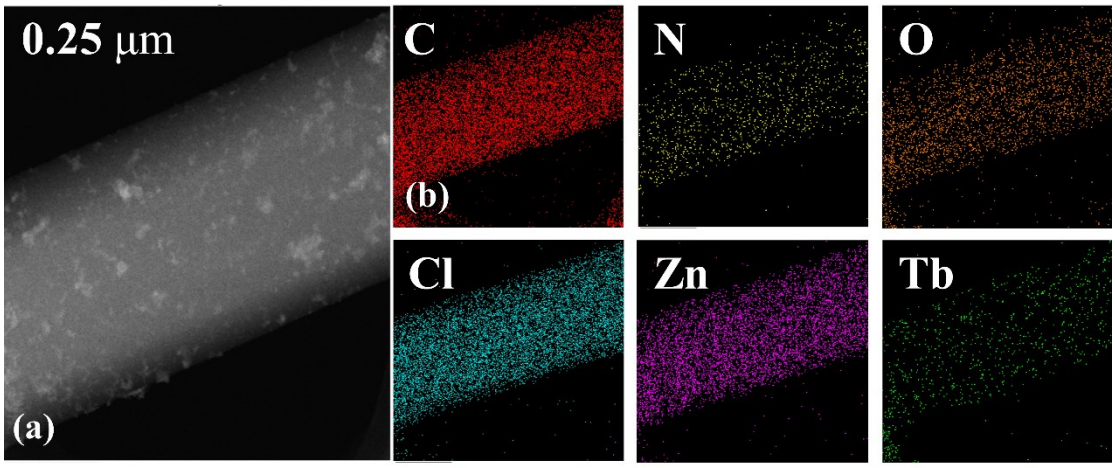

Fig. S21. (a) TEM image of **1**, (b) EDS-mapping images of C, N, O, Cl, Zn and Tb in **1** after sensing Tb^{3+} ions.